Proceedings of The Institute of Acoustics

FINITE ELEMENT ANALYSIS OF LOW FREQUENCY SONAR TRANSDUCERS

J.N. Decarpigny, J.C. Debus, B. Hamonic, R. Bossut
Laboratoire d'Acoustique *, Institut Supérieur d'Electronique du Nord,
41, boulevard Vauban, 59046 Lille Cedex, France.
P. Tierce, D. Morel
SINAPTEC S.A.R.L., 41, boulevard Vauban, 59800 Lille, France.
D. Boucher, B. Tocquet **
Groupe d'Etudes et de Recherches de Détection Sous-Marine,
Le Brusc, 83140 Six Fours les Plages, France.

INTRODUCTION

The finite element code **ATILA** has been specifically developed to aid the design of piezoelectric transducers, mainly for SONAR applications [1,2]. Thus, it is able to perform the modal analysis of both axisymmetrical and fully three-dimensional piezoelectric projectors. It can also provide their harmonic response under radiating conditions : nearfield and farfield pressure, transmitting voltage response, directivity pattern, electrical impedance. Finally, it can supply important information which concern their mechanical structure : displacement field, nodal plane positions, stress field and various stress criteria ... The aim of this paper is twofold. First, a brief description of the methods retained in the code is given. A particular emphasis is placed on the finite element approach which is used to solve the radiation problem and is related to monopolar [3,4] as well as dipolar dampers [5-7]. Second, several typical results are presented. They correspond to quite different structures and concern Tonpilz transducers [2,8,9], a deep submergence ring transducer [10,11] and a low frequency flextensional projector [12,13]. They demonstrate the actual abilities of the code, with respect to experimental results. In conclusion, present developments are described, with some details about the coupling with other approaches as well as the modelling of new materials.

DESCRIPTION OF THE METHOD

To model a radiating piezoelectric transducer using the **ATILA** code, the finite element mesh must include the structure as well as a part of the fluid domain [2,12]. The unknown fields are the displacement field $\underline{u}$ in the whole structure, the electrical potential φ in the piezoelectric material and the pressure field p in the fluid. The equations which have to be solved are, first, the equation of motion in the structure, second, the Poisson equation in the piezoelectric material and, third, the Helmholtz equation in the fluid. Kinematic and dynamic continuity equations between displacement and pressure fields are enforced on the interface, due to the variational formulation [2,4], and an appropriate damping condition [2-7] is applied to the spherical external surface Γ that surrounds the fluid domain. Then, the whole set of equations is, in matrix form [2,7,14] :

$$\begin{bmatrix} [K_{uu}] - \omega^2[M] & \underline{K}_{u\varphi} & -[L] \\ \underline{K}_{u\varphi}^T & K_{\varphi\varphi} & \underline{Q}^T \\ -\rho^2 c^2 \omega^2 [L]^T & \underline{Q} & [H] - \omega^2 [M_1] \end{bmatrix} \begin{bmatrix} \underline{U} \\ \varphi_0 \\ \underline{P} \end{bmatrix} = \begin{bmatrix} \underline{F} \\ -I/j\omega \\ \rho c^2 \underline{\Psi} \end{bmatrix} \qquad (1)$$

where :

- $\underset{\sim}{U}$, $\underset{\sim}{F}$, $\underset{\sim}{P}$ are vectors that contain the nodal values of the displacement field, the applied force and the pressure field,
- $\underset{\sim}{\Psi}$ is a vector that represents the outgoing flow through Γ,
- φ_0 is the applied voltage, while I is the entering current intensity,
- $[K_{uu}]$ and $[H]$ are the solid and fluid stiffness matrices,
- $[M]$ and $[M_1]$ are the solid and fluid mass matrices,
- $\underset{\sim}{K}_{u\varphi}$ and $K_{\varphi\varphi}$ result from the assembling of the piezoelectric and dielectric matrices, followed by a static condensation of the internal potential degrees of freedom,
- $[L]$ is the interface connectivity matrix,
- $\underset{\sim}{0}$ is a null vector,
- ρ and c are the fluid density and sound speed,
- ω is the circular frequency,
- T means transposed.

If a dipolar damping condition is applied on the external boundary Γ, $\underset{\sim}{\Psi}$ is given by [2-7] :

$$\underset{\sim}{\Psi} = -\frac{1}{\rho c}\left(\frac{1}{R} + j\frac{\omega}{c}\right)[D]\,\underset{\sim}{P} + \frac{1}{\rho c}\,\frac{\frac{1}{R} - j\frac{\omega}{c}}{1 + \frac{\omega^2 R^2}{c^2}}\,[D']\,\underset{\sim}{P} \qquad (2)$$

where R is the radius of Γ. $[D]$ and $[D']$ are obtained by assembling simple surface elements from Γ. The first term is the monopolar contribution associated with a spherical wave impedance and the second term is the dipolar contribution.

In the case of an in-air analysis, the third line and column of equation (1) are deleted. To obtain the resonance modes and frequencies, φ_0 and $\underset{\sim}{F}$ are then cancelled and the eigenvalues of the remaining matrix are computed. To obtain the antiresonance modes and frequencies, I and $\underset{\sim}{F}$ are cancelled and the new eigenvalues are computed. Finally, to obtain the harmonic response, $\underset{\sim}{F}$ is cancelled and $\underset{\sim}{U}$ and I are obtained for given values of φ_0 and ω. In the case of an in-water analysis, the whole system is solved with $\underset{\sim}{F}$ equal to zero, and $\underset{\sim}{U}$, I and $\underset{\sim}{P}$ are obtained for given values of φ_0 and ω.

If, in the case of an in-water analysis, only the monopolar term is retained in equation (2), it means that the external boundary Γ is in the farfield region. Then, with respect to spherical coordinates, the pressure p on Γ can be expressed by :

$$p(R,\theta,\varphi) = \frac{e^{-jkR}}{kR}\,F_0(\theta,\varphi) \qquad (3)$$

and the transmitting voltage response as well as the directivity pattern of

the modelled transducer are immediately obtained. However, the farfield conditions are often drastic [2,15] and require large fluid meshes. Thus, to overcome these difficulties and to allow a mesh size reduction, both monopolar and dipolar terms are generally retained and F_0 has to be deduced from a special extrapolation algorithm [6,7,16]. In fact, the exact radiated pressure field can be easily split following its multipolar expansion :

$$p(r,\theta,\varphi) = \frac{e^{jkr}}{kr} \sum_{n=0}^{\infty} \frac{F_n(\theta,\varphi)}{(jkr)^n} \qquad (4)$$

where F_n is deduced from F_{n-1} using a simple differential operator [5]. Then, restricting the problem to the axisymmetrical case, F_0 can be written :

$$F_0(\theta) = \sum_m a_m \cos m\theta \qquad (5)$$

and, the various components $F_n(\theta)$ being computed, the whole expression of $p(r,\theta)$ can be expanded in its various Fourier components. So, a limited multipolar expansion is obtained from a limited set of a_m coefficients, which has to be explicitely identified from the nodal values of the pressure inside Γ. Finally, knowing the a_m values, the farfield is completely described.

Before concluding this section, it is interesting to point out the special case of a long ceramic stack. In this case, the motion of the stack, as well as the motion of the tailmass if it exists, is often a simple dilational motion. So, the stack can be modelled using the classical transfer matrix approach. Then, the interface between the stack and the remaining part of the structure is assumed to have a plane motion and only this remaining part has to be described by a finite element mesh. Thus, the second line and column of equation (1) have to be deleted, $\underline{F}$ being straightforwardly deduced from the transfer matrix equations with respect to the applied potentials and the frequency [1]. This mixed plane wave - finite element approach has proved to be really successful in a lot of examples.

DESCRIPTION OF TYPICAL RESULTS

Modal analysis of a Tonpilz transducer

The first example is a classical Tonpilz transducer (figure 1) which has to be modelled using a fully three-dimensional finite element mesh. This mesh describes only one quarter of the structure and contains 115 elements, 597 nodes and nearly 1200 degrees of freedom. Numerical results are displayed in Table 1, while figure 2 presents the displacement fields associated with three flexural modes of the headmass. Mode identification was experimentally obtained using Chladni's method, which clearly demonstrated the accuracy of the theoretical mode shapes. Moreover, keeping in mind the large size of the numerical problem and the absence of adjusted parameters, the results in Table 1 are quite good.

Mode number	f(FEM)	f(exp)	Mode identification
1	1.00	0.98	first dilational mode
2	1.96	1.77	first headmass flexural mode
3	2.19	1.98	second headmass flexural mode
4	2.47	-	first tailmass mode
5	3.03	2.82	second dilational mode
6	3.66	3.35	third headmass flexural mode

Table 1. Resonance frequencies of the first Tonpilz transducer. Values are scaled down to the value of the first FEM mode frequency.

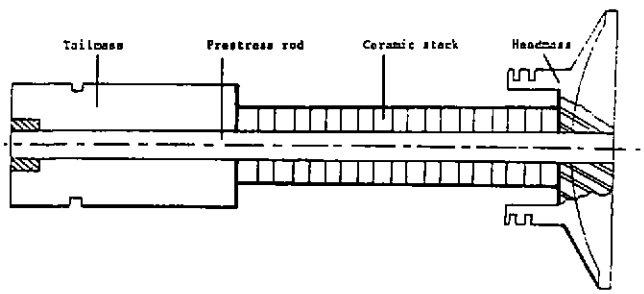

Figure 1. Schematic description of the first Tonpilz transducer

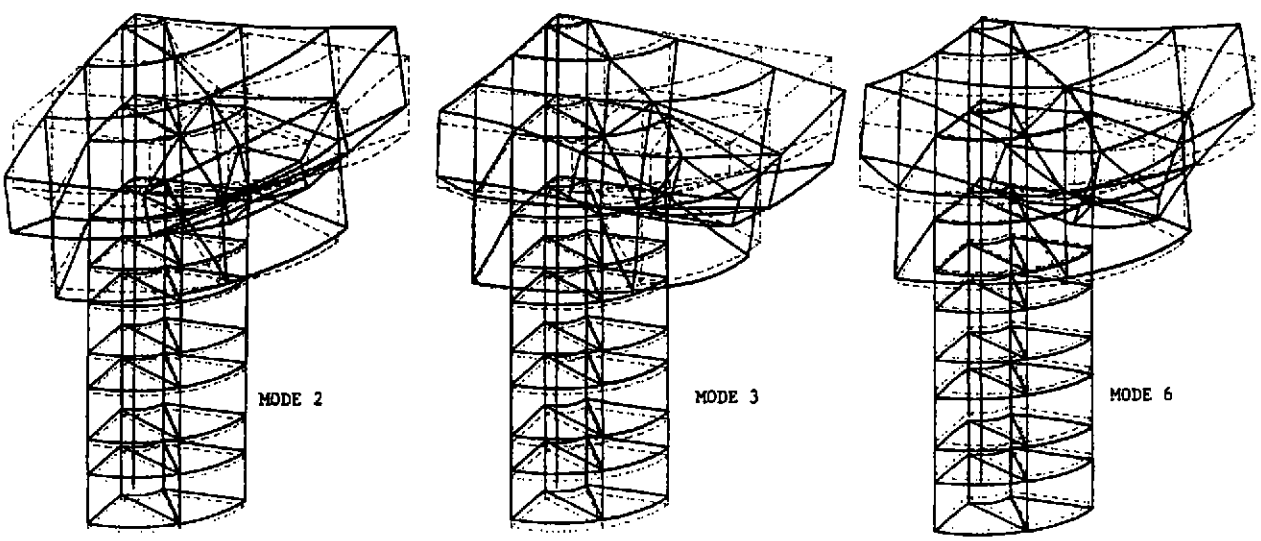

Figure 2. Displacement field of the headmass for modes 2, 3 and 6.

Modal analysis of a ring transducer

The second example is a special deep submergence transducer which is composed of a thick ring with ten small Tonpilz radially fastened to its inside face (figure 3). Assuming an identical electrical excitation of the ten ceramic stacks, the finite element mesh can be reduced to one quarter of an 18 degrees sector. This mesh contains 50 elements, 327 nodes and nearly 800 degrees of freedom. Numerical results are displayed in Table 2, while figure 4 presents the displacement fields associated with the second and third modes. Here again, the accuracy is correct and the theoretical mode shapes were experimentally asserted.

Mode number	f(FEM)	f(exp)	mode identification
1	1.00	0.99	ring radial mode
2	3.74	3.58	first Tonpilz dilational mode
3	5.91	5.57	ring ovalization mode
4	7.54	6.48	first tailmass mode
5	8.30	7.47	ring circumferential mode

Table 2. Resonance frequencies of the ring transducer. Values are scaled down to the value of the first FEM mode frequency.

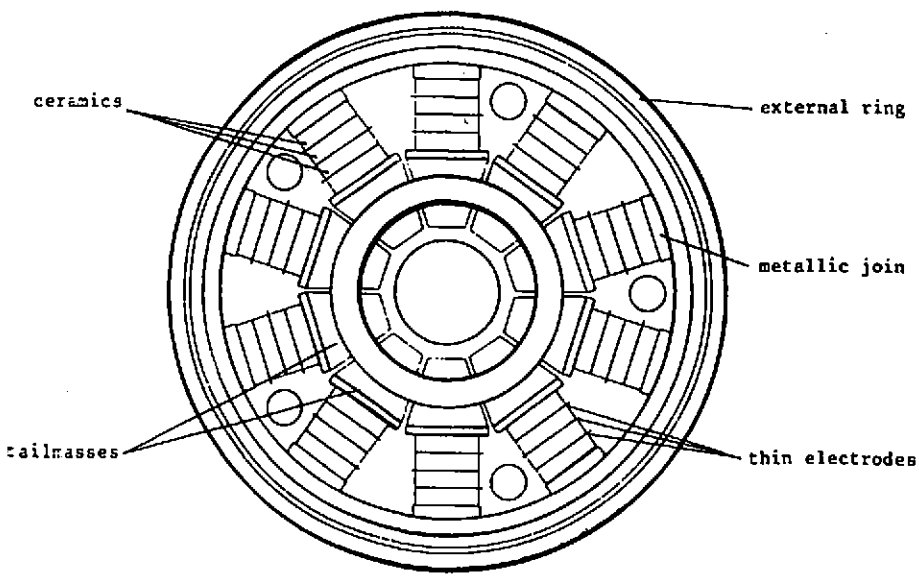

Figure 3. Schematic description of the ring transducer.

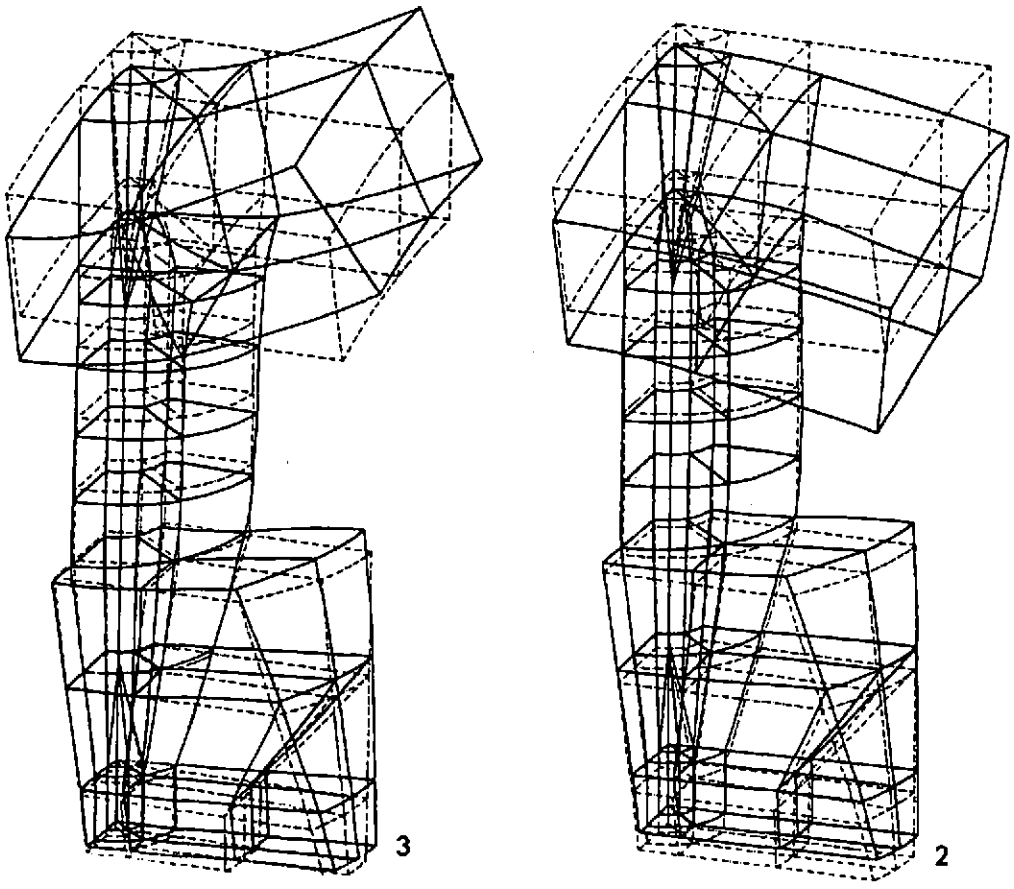

Figure 4. Displacement field of the ring transducer for modes 2 and 3.

Harmonic analysis of a radiating Tonpilz transducer

The third example is an axisymmetrical Tonpilz transducer which is radiating in water. The finite element mesh is described on figure 5. Due to the simple behaviour of the radiated acoustic wave, only monopolar dampers are retained on Γ. The transmitting voltage response T_v of the transducer was computed and measured for several different electrical excitations of the ceramic stack [9]. Figure 6 displays the variation of this response, versus reduced frequency, for a special voltage shading which corresponds to a very large measured transducer efficiency across the whole frequency range. A nice agreement is obtained, which allows a powerful analysis of the main features of this curve (maxima, minima) in terms of mechanical effects (resonance, new nodal plane entering ...) [2,9]. The same accuracy was always obtained with respect to the frequency spectrum for all the Tonpilz transducers we studied. However, in some cases, less accuracy was obtained with respect to the level, due to low values of the transducer efficiency. In these cases, material losses have to be modelled to overcome the discrepancy.

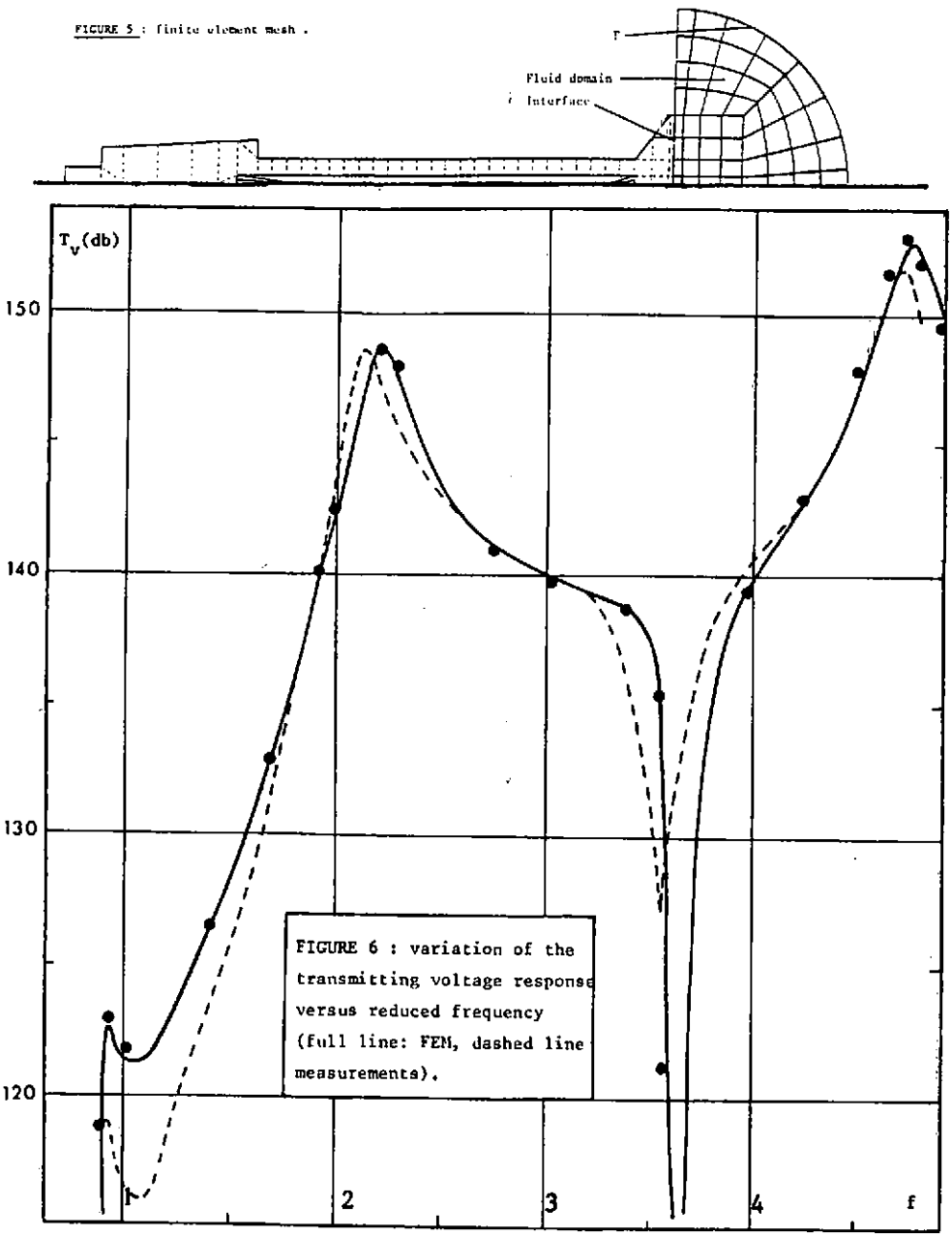

FIGURE 6 : variation of the transmitting voltage response versus reduced frequency (full line: FEM, dashed line measurements).

Harmonic analysis of a radiating flexural shell transducer

This final example is an axisymmetrical flexural shell transducer which is described on figure 7. The analysis was performed using thin shell elements, the mixed plane wave-finite element approach, and dipolar dampers upon the external boundary Γ, which was assumed to be well inside the nearfield [12,13]. First, the transmitting voltage response is displayed, versus reduced frequency, on figure 8. Apart from a slight upward shift of the curve at the upper limit of the range, which can be explained by the coarseness of the mesh with respect to the wavelength in this limit, the agreement is nice. Figure 9

gives the directivity patterns for three frequencies. It compares the experimental results, the finite element results before and after the extrapolation and, finally, the results obtained from an exterior Helmholtz integral formulation [17], using as input the transducer displacement field which was produced by the finite element computation. Beyond their accuracy, these results demonstrate clearly the efficiency of the extrapolation method to provide farfield quantities.

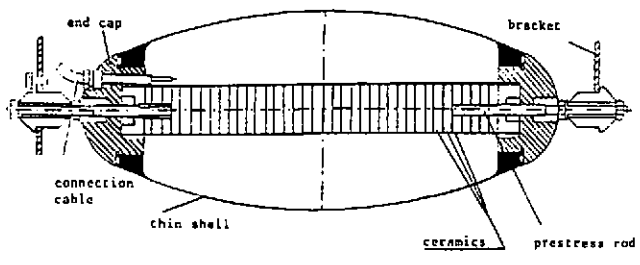

FIGURE 7 : schematic description of the flextensional transducer.

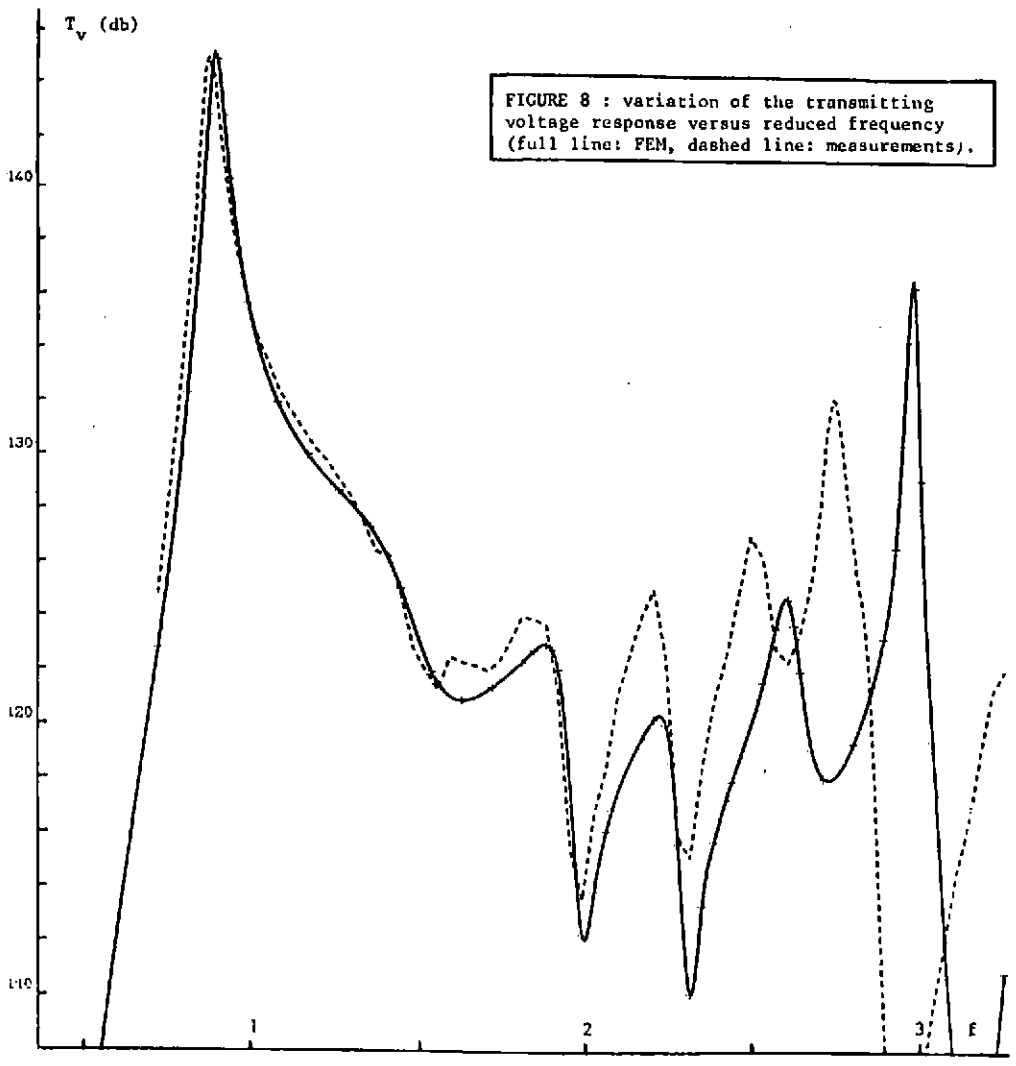

FIGURE 8 : variation of the transmitting voltage response versus reduced frequency (full line: FEM, dashed line: measurements).

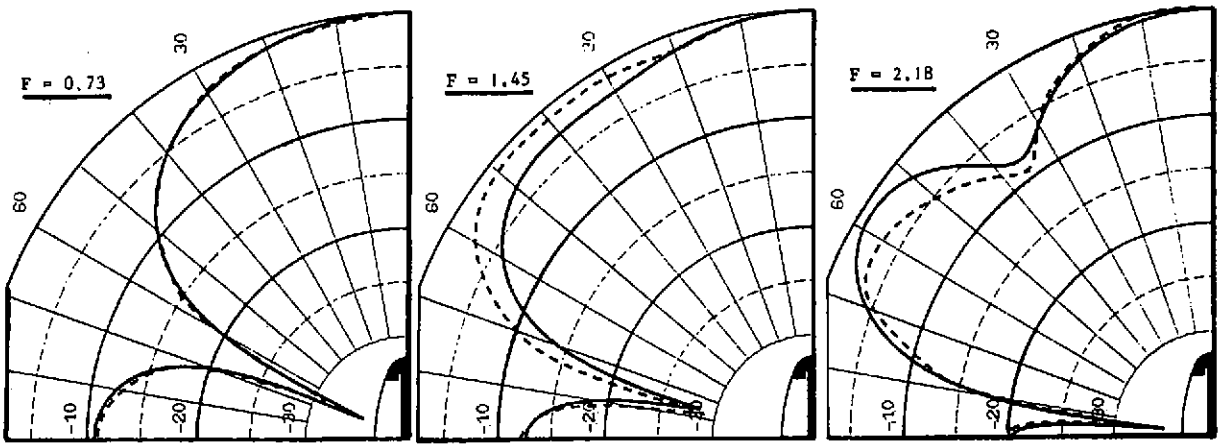

Figure 10a. Directivity patterns, normalized to the same value. Full line : FEM with extrapolation. Dashed line : measurements.

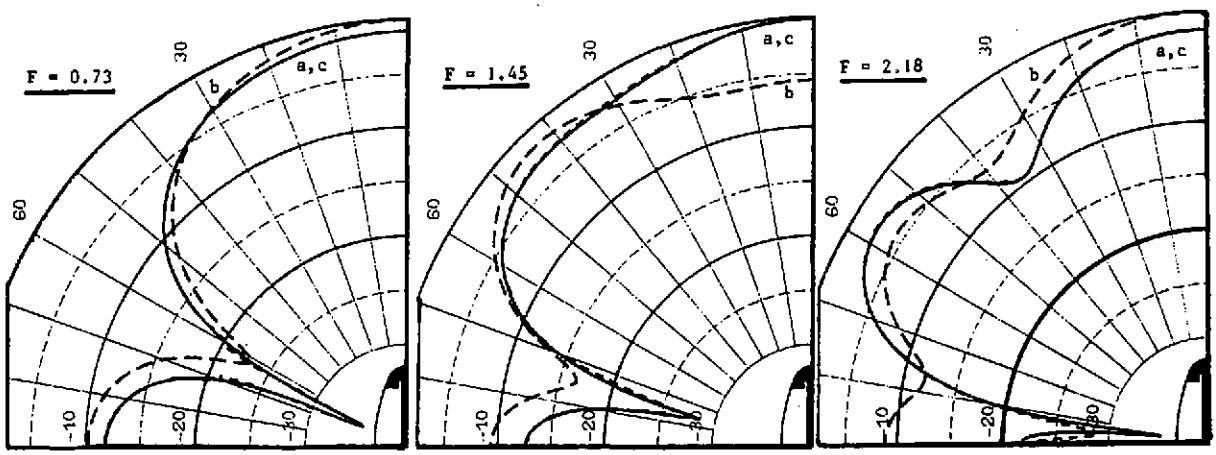

Figure 10b. Directivity patterns (without normalization). Full line (a) : FEM with extrapolation. Dashed line (long dashes (b)) : FEM without extrapolation. Dashed line (short dashes (c)) : Helmholtz integral equation.

CONCLUSION

The previous examples actually prove the ability of the ATILA code to model various kinds of piezoelectric sonar projectors. However, several new developments are currently under test to improve it. They concern mainly the *modelling of material losses*, to allow an accurate description of low efficiency structures as well as of various new materials (viscoelastic materials, new polymer and composite ceramics ...), *the coupling between a finite element modelling of the structure and an Helmholtz integral formulation of the radiation problem* [17], such as to reduce drastically the

mesh sizes, *the coupling between a finite element modelling of the structure and simple approximate radiation models*, and, finally, the *creation of new elements* (GRP elements ...). This code has been in current use for three years to help the design of new transducers, mainly for sonar but also for macrosonics applications.

REFERENCES

* U.A. 253 - C.N.R.S.

** Now with THOMSON-SINTRA DASM, Chemin des Travails, 06800 Cagnes sur Mer, France.

[1] J.N. Decarpigny, J.C. Debus, B. Tocquet, D. Boucher, J. Acoust. Soc. Am., 78, 1499, (1985).

[2] J.N. Decarpigny, Doctoral Thesis, Lille University, (1984).

[3] D.V. Dean, Doctoral Thesis, Postgraduate Naval School, Monterey, (1970).

[4] O.C. Zienkiewicz, R.F. Newton, Proceedings of the Symposium on finite element techniques, Stuttgart, (1969).

[5] A. Bayliss, M. Gunzburger, E. Turkel, ICASE report N80/1, NASA Langley, (1980).

[6] R. Bossut, J.N. Decarpigny, Communication M4, 106th ASA meeting, San Diego, (1983).

[7] R. Bossut, Doctoral Thesis, Valenciennes University, (1985).

[8] J.N. Decarpigny, J.C. Debus, B. Tocquet, D. Boucher, Communication KK1, 102th ASA meeting, Miami, (1981).

[9] J.N. Decarpigny, J.C. Debus, P. Tierce, D. Boucher, B. Tocquet, Communication L9, 112th ASA meeting, ANAHEIM, (1986).

[10] D. Boucher, B. Tocquet, J.C. Debus, P. Tierce, Communication WW7, 106th ASA meeting, San Diego, (1983).

[11] P. Tierce, Doctoral Thesis, Valenciennes University, (1985).

[12] B. Hamonic, J.C. Debus, J.N. Decarpigny, D. Boucher, B. Tocquet, International Symposium on practical aspects in the computation of shell and spatial structure, Leuven, (1986).

[13] B. Hamonic, J.C. Debus, J.N. Decarpigny, D. Boucher, B. Tocquet, Communication L4, 112th ASA meeting, ANAHEIM, (1986).

[14] J.T. Hunt, M.R. Knittel, D. Barach, J. Acoust. Soc. Am., 55, 269, (1974).

[15] R.J. Bobber, 'Underwater electroacoustic measurements', NRL Report, D.T.I.C. Dpt. of Defense, USA, (1970).

[16] R. Bossut, J.N. Decarpigny, B. Tocquet, D. Boucher, Communication X8, 111th ASA meeting, Cleveland, (1986).

[17] B. Stupfel, A. Lavie, to be published (1987).